nique will be most useful in cases in which the residues of importance are rare in the sequence or whose resonances are resolved from those of like residues because of protonation, metal ligation, hydrogen bonding, or other interactions that lead to unusual chemical shifts.

ACKNOWLEDGMENTS

We thank Dr. P. F. Weaver for providing the culture of *R. rubrum* strain G-9 and for his advice concerning growth conditions. We also thank Dr. R. G. Bartsch for his helpful advice.

Registry No. RuBPCase, 9027-23-0; cyt c_2, 9035-43-2; cyt c', 9035-41-0; NH_4^+, 14798-03-9; ^{15}N, 14390-96-6.

REFERENCES

Abragam, A. (1961) *The Principles of Nuclear Magnetism*, Oxford University Press, London.
Anderson, L. E. (1975) *Adv. Enzymol. Relat. Areas Mol. Biol. 42*, 457–461.
Bachovchin, W. W., & Roberts, J. D. (1978) *J. Am. Chem. Soc. 100*, 8041–8047.
Bartsch, R. G. (1978) in *The Photosynthetic Bacteria* (Clayton, R. K., & Systrom, W. R., Eds.) Plenum Press, New York.
Bax, A. (1984) *Two-Dimensional Magnetic Resonance in Liquids*, Delft University Press, Reidel, Boston.
Bothner-By, A. A., & Gassend, R. (1973) *Ann. N.Y. Acad. Sci. 222*, 668–675.
Carr, H. Y., & Purcell, E. M. (1954) *Phys. Rev. 94*, 630–638.
Coates, H. B., McLachlan, K. A., Campbell, I. D. & McColl, C. E. (1973) *Biochim. Biophys. Acta 310*, 1–10.
Griffey, R. H., Poulter, C. D., Bax, A., Hawkins, B. L., Yamaizumi, Z. W. W., & Nishimura, S. (1983) *Proc. Natl. Acad. Sci. U.S.A. 80*, 5895–5897.
Griffey, R. H., Redfield, A. G., Loomis, R. E. W. W., & Dahlquist, F. W. (1985) *Biochemistry 24*, 817–822.
Gust, D., Moon, R. B., & Roberts, J. D. (1975) *Proc. Natl. Acad. Sci. U.S.A. 72*, 4696–4700.
Hahn, E. L. (1950) *Phys. Rev. 80*, 580–594.
Jardetzky, O. (1981) *Acc. Chem. Res. 14*, 291–298.
Kalk, A., & Berendsen, H. J. C. (1976) *J. Magn. Reson. 24*, 343–366.
Kanamori, K., & Roberts, J. D. (1983) *Acc. Chem. Res. 16*, 35–41.
Markley, J. L. (1975) *Acc. Chem. Res. 8*, 70–80.
Mason, J. (1981) *Chem. Rev. 81*, 205–227.
McArthur, D. A., Hahn, E. L., & Walstedt, R. E. (1969) *Phys. Rev. 188*, 609–638.
Morishima, I., & Inubushi, T. (1977) *FEBS Lett. 81*, 57–60.
Morris, G. A., & Freeman, R. (1979) *J. Am. Chem. Soc. 101*, 760–762.
Ormerod, J. G., Ormerod, J. D., & Gest, H. (1961) *Arch. Biochem. Biophys. 94*, 449–463.
Roberts, J. D. (1980) *Rice Univ. Stud. 66*, 147–178.
Schloss, J. V., Phares, E. F., Long, M. V., Norton, L. I.; Stringer, C. D., & Hartman, F. C. (1979) *J. Bacteriol. 137*, 490–501.
Sogn, J. A., Gibbons, W. A., & Randall, E. W. (1973) *Biochemistry 12*, 2100–2105.
Vold, R. L., Waugh, J. S., Kline, M. P., & Phelps, D. E. (1968) *J. Chem. Phys. 48*, 3831–3832.
Werebelow, L. G., & Marshall, A. G. (1973) *J. Am. Chem. Soc. 95*, 5132–5134.
Witanowski, M., Stefaniak, L., & Webb, G. A. (1981) *Annu. Rep. NMR Spectrosc. 11B*, 1–502.
Woessner, D. E. (1962) *J. Chem. Phys. 37*, 647–654.

Triplet-State Detection of Labeled Proteins Using Fluorescence Recovery Spectroscopy

Alan F. Corin,[‡] Edward Blatt,[§] and Thomas M. Jovin*
Abteilung Molekulare Biologie, Max-Planck-Institut für Biophysikalische Chemie, D-3400 Göttingen, FRG
Received February 21, 1986; Revised Manuscript Received December 15, 1986

ABSTRACT: The experimental procedures for detecting the triplet states of chromophores in solutions (cuvettes) by fluorescence recovery spectroscopy (FRS) are described in detail, together with applications in studies of protein structure and protein–cell interactions in the microsecond to millisecond time domain. The experimental configuration has been characterized by measuring the emission intensities and anisotropies of eosin and erythrosin immobilized in poly(methyl methacrylate). The fluorescence data are compared with those from phosphorescence emission measurements and with theoretical predictions. Triplet-state lifetimes were obtained in 5 mM phosphate buffer, pH 7.0, of concanavalin A labeled with eosin, tetramethylrhodamine, and fluorescein and of α_2-macroglobulin labeled with the first two probes. In the case of labeled concanavalin A, iodide quenching measurements gave bimolecular rate constants of approximately 10^9 M^{-1} s^{-1}. The usefulness of FRS for studying protein–cell interactions is exemplified with eosin-labeled concanavalin A bound to living A-431 human epidermoid carcinoma cells. Finally, the advantages and disadvantages of the technique are compared to those of the alternative phosphorescence emission method.

The fluorescence properties of small molecules are of great utility in the elucidation of macromolecular dynamics and structure (Rigler & Ehrenberg, 1976). This has been particularly true over the past two decades, in which developments in computer and laser technology have enhanced experimental capabilities. More recently, the excited triplet states of appropriate probe molecules have been exploited since their emission processes occur over time scales comparable to protein rotation in larger complexes and in membranes (Cherry, 1978;

[‡]Present address: Life Sciences Research Laboratories, Eastman Kodak Company, Rochester, NY 14650.
[§]Present address: Division of Applied Organic Chemistry, CSIRO, Melbourne, Victoria 3001, Australia.

0006-2960/87/0426-2207$01.50/0

Jovin et al., 1981; Matayoshi et al., 1983; Corin et al., 1985; Hoogevest et al., 1985).

To date, the two most common methods of triplet-state detection have utilized absorption (Cherry, 1978, 1979; Austin et al., 1979) and phosphorescence emission (Austin et al., 1979; Garland & Moore, 1979; Jovin et al., 1981) processes. A third technique, originally applied in the microscope and termed fluorescence depletion (Johnson & Garland, 1981, 1982; Garland & Johnson, 1985) and in a more recent implementation of a microscope-based system denoted as polarized fluorescence depletion (Yoshida & Barisas, 1986), measures the photoselective depletion of the ground state by monitoring the return of the polarized fluorescence intensity to the initial steady-state values. The technique combines the high sensitivity of steady-state fluorescence measurements with the relatively long triplet-state lifetime. Furthermore, a variety of familiar fluorescent probes can be used.

In this paper, we present a detailed description of the experimental procedures for detecting the triplet states of fluorescence molecules conjugated to proteins in solution or suspension by the method of fluorescence recovery spectroscopy (FRS).[1]

Materials and Methods

Materials. Carboxyeosin (CarEo), erythrosin 5′-isothiocyanate (ErITC), eosin 5′-isothiocyanate (EITC), and fluorescein 5′-isothiocyanate (FITC) were purchased from Molecular Probes (Junction City, OR), and tetramethylrhodamine 5′-isothiocyanate (TMRITC) was purchased from Polysciences (Warrington, PA). Methyl methacrylate and 2,2′-azobis(2-methylpropanenitrile), supplied by Merck (Darmstadt, FRG), were used to make solid solutions of CarEo and ErITC in poly(methyl methacrylate) (PMMA) according to the method outlined by Garland and Moore (1979). NaI and NaCl (both from Merck) and $Na_2S_2O_3$ (Sigma, St. Louis, MO) were used as supplied.

The following fluorescent derivatives of jack bean concanavalin A (conA) (Sigma) were prepared according to Chan et al. (1979) and Austin et al. (1979): EITC–conA, TMRITC–conA, and FITC–conA. The labeling ratios were 1.2, 1.4, and 3 probes per conA tetramer, respectively.

The fluorescent derivatives of α_2-macroglobulin, EITC–α_2M and TMRITC–α_2M, were prepared according to Chan et al. (1979).

All buffer solutions were 5 mM sodium phosphate, pH 7.0. For the I^- quenching measurements, a constant ionic strength was maintained by addition of NaCl (Merck) containing 0.1 mol % $Na_2S_2O_3$ (Merck) to prevent I_3^- formation (Lehrer, 1971; Barboy & Feitelson, 1985).

Suspensions of cells labeled with EITC–conA were diluted to (1–3) × 10^6 cells/mL.

Experimental Design for FRS Measurements. In FRS experiments, steady-state fluorescence emission is first established by a continuous-wave (CW) laser light source. Population of the triplet state is then achieved with a second, more intense (actinic) laser pulse. The resulting depletion in the ground-state population is observed as a decrease in the steady-state fluorescence. The ground-state population then recovers to the prepulse light level with a time course determined by the triplet-state lifetime.

A number of optical configurations are available for collection of FRS signals (Johnson & Garland, 1981, 1982; Wegener & Rigler, 1984; Wegener, 1984; Yoshida & Barisas, 1986; Szabo et al., unpublished results). In the general case with 90° detection and small-aperture collection optics, two adjustable polarizers are necessary (Wegener, 1984; Szabo et al., unpublished results). The work presented here was mainly concerned with the experimental design for the determination of triplet-state lifetimes. Thus, we chose a simpler configuration that is effective when the chromophore either is immobilized or rotates freely in solution with correlation times in the submicrosecond region, i.e., when the anisotropy is time-independent.

Figure 1 shows the experimental features of the depletion technique. The arrangement is an extension of a phosphorescence spectrometer design described in previous publications (Austin et al., 1979; Matayoshi et al., 1983; Corin et al., 1985). For most samples, the 514-nm line of a Coherent (Palo Alto, CA) Model 90 INNOVA continuous-wave argon ion laser is used to stimulate steady-state fluorescence. In the case of fluorescein derivatives, the 488-nm line is used. The beam is directed through a Spectra Physics (Palo Alto, CA) Model 310-21 double-rhomb rotating polarizer, which is adjusted such that the plane of polarization of the CW beam is 90° with respect to the plane of polarization of the dye laser. This arrangement matches the steady-state fluorescence intensities of the two emission polarization states (see below). A Lambda Physik (Göttingen, FRG) Model EMG50 excimer laser operating with the XeCl line at 308 nm pumps a dye laser yielding 10-ns pulses of vertically polarized light. Approximately 2 mJ/pulse of visible light tunable between 500 and 520 nm is obtained with Coumarin 307 (Lambda Physik) as the laser dye. The excitation wavelength was 520 nm for all experiments except those with the FITC conjugate, in which case 500 nm was used. In order to achieve a detectable degree of depletion, a relatively high energy density is required in the pump beam and the two beams must coincide as they pass through the sample. Several optical arrangements may be utilized; the one we adopted in the present study is shown in Figure 1. The dye and argon laser outputs are each focused independently by 30- and 100-cm focal length lenses, respectively, in order to match the beam shapes. Spatial coincidence of the beams is obtained by steering the argon beam to a Melles Griot (Irvine, CA) 03 BPL pellicle beam splitter mounted in an NRC (Fountain Valley, CA) gimbal optical mount placed between the dye laser and the sample chamber. The uncoated, <5 μm thick pellicle beam splitter transmits 92% and reflects 8% of the incident dye laser beam toward the sample chamber. (One advantage of such a configuration is the greater stability of the argon laser achieved through operation at relatively high power levels.) A third lens focuses the two beams in order to obtain a beam spot diameter of ~0.2 mm at the center of the cuvette.

An estimate of the change in temperature of the solution brought about by the pulsed laser can be calculated as follows. The beam is assumed to follow a cylindrical pathway through the solution, forming a volume element comprising a known mass of water. To obtain an upper limit for the temperature rise, it is assumed that all the absorbed light energy is converted into heat. Using the extinction coefficient of the dye (Johnson & Garland, 1982), we calculate temperature rises of 0.001, 0.05, and 0.18 °C under our experimental conditions for the EITC, TMRITC, and FITC derivatives in buffer,

[1] Abbreviations: FRS, fluorescence recovery spectroscopy; PMMA, poly(methyl methacrylate); conA, concanavalin A; α_2M, α_2-macroglobulin; CarEo, carboxyeosin; EITC, eosin 5′-isothiocyanate; TMRITC, tetramethylrhodamine 5′-isothiocyanate; ErITC; erythrosin 5′-isothiocyanate; FITC, fluorescein 5′-isothiocyanate; SNR, signal-to-noise ratio; Φ_f, fluorescence quantum yield; Φ_t, quantum yield for intersystem crossing; CW, continuous wave; TTL, transistor–transistor logic; COT, cyclooctatetraene.

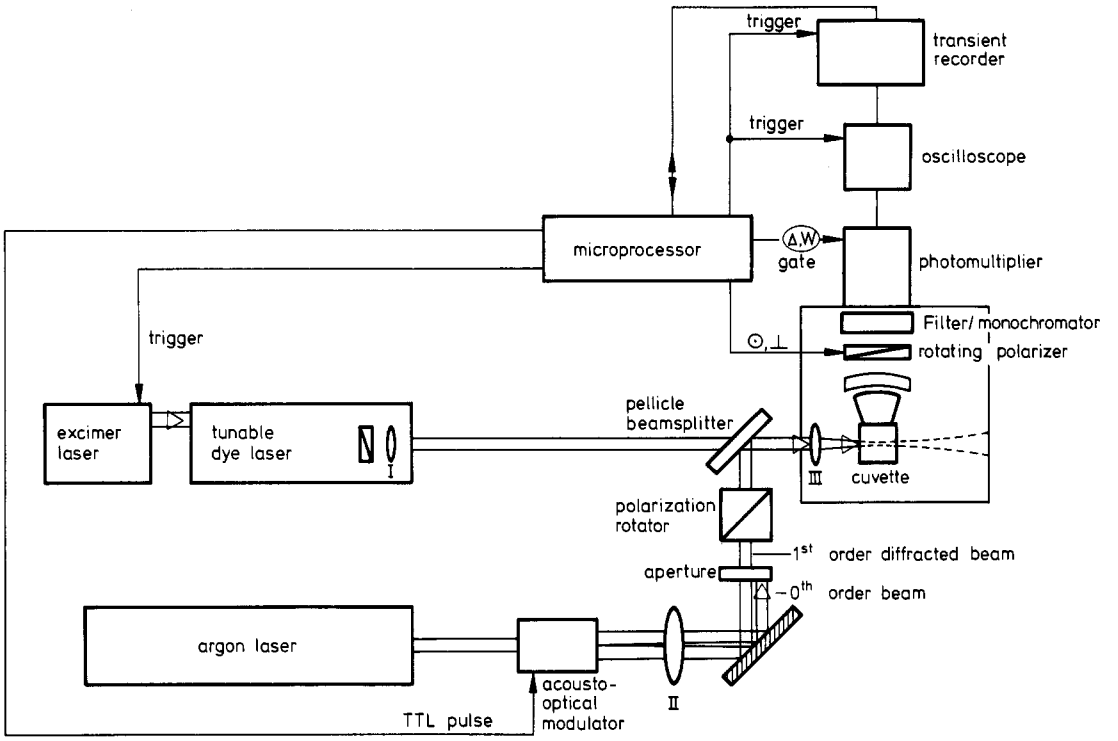

FIGURE 1: Schematic of the triplet-state spectrometer. Symbols: Δ, adjustable delay; W, variable width; ⊙ and ⊥, parallel and perpendicular orientations of the polarizer, respectively; I, II, and III, biconvex lenses with focal points at 30, 100, and 24 cm, respectively. The three trigger signals to the excimer laser, the photomultiplier gating curcuit, and the transient recorder and the digital (TTL) pulses to the acoustooptical modulator and the stepping motor controlling the rotation of the emission polarizer are generated directly from the microprocessor. See text for more details on components and sequence of operation.

respectively. With the exception of FITC, the worst case situation, temperature rises are negligible. As pointed out by Johnson and Garland (1982), probes with fluorescence quantum yields (Φ_f) approaching unity will release only a fraction of the energy as heat because of the longer emission wavelength. Thus, for FITC ($\Phi_f \sim 0.9$; Parker, 1968), the temperature rise will be less than the value given above.

The following construction and procedures facilitated system alignment before each set of experiments. The temperature-jacketed sample chamber is built into a larger rectangular enclosure. The dye laser beam passes through apertures placed at either end of the enclosure and is projected onto a wall some distance from the box. The argon laser is steered through the same path with the use of a mirror and the pellicle beam splitter. The third focusing lens is placed after the beam splitter. To view the focused beam at the sample, a thin glass plate is placed in the sample chamber at an angle of ~45° to the incoming beams. A portion of the laser beams is thus deflected onto a surface at 90° with respect to the incident light. A 5-cm focal length lens focuses the two images deflected from the front and back surfaces of the plate. The double image is used to assess the degree of which the beams are concentric at the center of the cuvette and to adjust the beam splitter accordingly.

The fluorescence is detected at right angles to the excitation sources by an EMI (Hayes, U.K.) 9817 QGB photomultiplier tube (PMT). The photocurrent is amplified by a plug-in unit (Model 7A22 or 7A15A) of a Tektronix (Beaverton, OR) Model 7603 oscilloscope. The photomultiplier is electronically gated in order to suppress excessive photocurrents which could result from the very intense prompt fluorescence excited by the pulsed beam (Jovin et al., 1981). The two polarized components of the emitted light are alternatively selected by rotating a sheet polarizer 90° after a preselected number of laser flashes. Optical filters [potassium dichromate solution, appropriate glass cutoff filters (such as KV550, Schott, Mainz, FRG) and/or narrow band-pass filters (Corion, Holliston, MA)] are inserted between the sample chamber and the PMT to isolate the fluorescence from the scattered laser light and from the phosphorescence emission. Neutral density filters in the path of the actinic source are used when necessary. As previously described (Corin et al., 1985), data records consisting of up to 1024 (but usually 512) channels of the two polarized components of emitted light are time averaged by strobing the contents of a Biomation 8100 (Palo Alto, CA) transient recorder into a microprocessor system after each pulse.

In order to obtain the true fluorescence recovery response of the probe molecule, two blank records are collected, summed, and subtracted from each sample data file. A detailed schematic of the data collection sequence is shown in Figure 2. The on/off state of both lasers is controlled by a microprocessor. Irradiation of the sample by the argon laser is minimized by directing the beam through a Coherent Model 308 acoustooptical modulator which is activated by a Coherent Model 418D digital driver and thereby serves as a fast optical shutter. A pulse delivered to the driver at a selected time before the dye laser is pumped turns on the first-order diffracted beam of the argon laser and induces the steady-state sample fluorescence (Figure 2). The zero-order beam is stopped by an aperture placed in the optical path. At the end of each transient curve the driver and, consequently, the first-order diffracted beam are turned off. In this manner the sample is spared irradiation during output strobing of the transient recorder and during periods when the emission polarizer is being rotated by 90°. Data are collected in the following real time sequence: (A) In a typical experiment 128 records of the fluorescence recovery are collected for the emission polarizer positioned first in the vertical position and then in the horizontal position (the orientations are relative

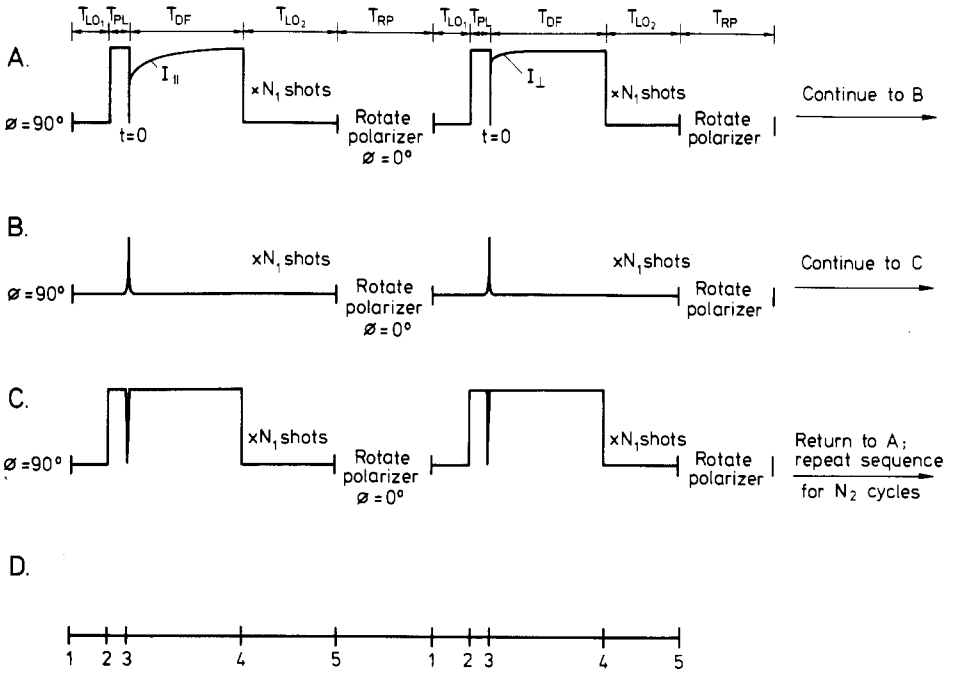

FIGURE 2: A schematic of the idealized real time data-collection sequence. (A) Collection of the parallel and perpendicular components of the fluorescence emission during a fluorescence recovery experiment. The following abreviations describing the sequence of time events (top row) are used: T_{LO_1} (light off 1); T_{PL} (prepulse light), argon laser is turned on, resulting in a steady-state fluorescence signal; T_{DF} (depletion of the fluorescence), recovery of the fluorescence after a depleting pulse; T_{LO_2} (light off 2), argon light is turned off; T_{RP} (rotation of polarizer), emission polarizer is rotated 90°; time zero ($t = 0$) coincides with the laser flash and refers to the beginning of depletion; $I_\parallel$ and $I_\perp$, polarized emission components oriented parallel and perpendicular, respectively, to the polarization direction of the actinic laser beam. (B) Subtract file 1 with only the dye laser pulsing. The argon laser is never turned on (i.e., the modulator is not pulsed). All else is the same as in (A). (C) Subtract file 2 with the argon laser light turned onto the sample and no pulsing of the dye laser. All else is the same as in (A). (D) Time progression of commands from the microprocessor defining the events in (A): (1) Set polarizer to the vertical position and begin data collected by sending a trigger to the oscilloscope and the transient recorder; (2) send TTL logic pulse to the modulator and turn on the argon laser light; (3) send trigger to the gate then to the excimer laser, causing dye laser to pulse (this is experimental time zero); (4) stop data collection and strobe the contents of the biomation into the microprocessor; (5) send TTL pulses to the stepping motor to rotate the polarizer 90°.

to the vertical polarization state of the actinic beam); (B) sequence A is repeated a second time in the absence of CW argon laser light; and (C) sequence A is repeated a third time in the absence of dye laser light pulses. (The records collected according to the procedures in (B) and (C) constitute the blank records.) The entire process is then repeated many times and averaged. Such a cyclic data-collection format provides a good control for variations in the lasers and instrumentation, effectively matching instrumental conditions during both sample data collection and blank subtract data collection.

In FRS experiments, $I_\parallel$ and $I_\perp$ are the polarized components of the emission for the analyzer set parallel and perpendicular to the actinic laser beam polarization, respectively. For phosphorescence, $I_\parallel$ and $I_\perp$ have their usual meaning (Jovin et al., 1981). The intensity profiles are corrected for overall gain inequalities between the two polarized components and for the finite emission aperture as previously described (Austin et al., 1979).

The time-dependent polarized light components are combined to form the functions $S(t) = I_\parallel(t) + 2I_\perp(t)$ and, where appropriate, $r(t) = [I_\parallel(t) - I_\perp(t)]/S(t)$; in the FRS measurement, $r(t)$ is an apparent anisotropy function. $S(t)$ represents either the phosphorescence intensity or the fluorescence depletion signal. An extensive treatment of the time dependence of the polarized components of the emitted light in the general case will be presented elsewhere (Szabo et al., unpublished results). When no depolarization occurs, the above-outlined expressions for $S(t)$ and $r(t)$ can be used and the time-independent anisotropy for an immobilized chromophore reduces to

$$r_0 = 2P_2(\cos \delta_{AE})/[7 - 2P_2(\cos \delta_{AE})] \qquad (1)$$

where δ_{AE} is the angle between the absorption and emission dipoles, and $P_2(X) = (3x^2 - 1)/2$ is the second Legendre polynomial. Equation 1 results from the general expression for the fluorescence intensity formulated in terms of the orientations of the actinic and monitoring beams and the emission analyzers and from the orientational correlation functions corresponding to the absorption and emission transition moments (Szabo et al., unpublished results). It is worth noting that the maximum possible anisotropy both for direct observation of delayed luminescence and for FRS is 0.4 under our geometric arrangement.

The data were transferred to an LSI-11/73 (DEC, Maynard, MA) and subjected to regression analysis. A least-squares Marquardt fitting procedure was used to fit the $S(t)$ decay according to

$$S(t) = S_0 \sum_{i=1}^{N} \alpha_i e^{-t/\tau_i} + B \qquad N \leq 3 \qquad (2)$$

where S_0 is proportional to the total population of the triplet state at $t = 0$ (i.e., after the laser flash), α_i is the fractional contribution of component i with decay time τ_i, and B is a time-invariant term.

Steady-state fluorescence polarization measurements were made either in a spectrofluorometer (SLM, Urbana, IL) or in the triplet-state spectrometer with the CW argon laser as the steady-state excitation source.

Results and Discussion

Summary of Photophysical Properties of the Probes. The photophysical properties of the long-lived triplet states of luminescent probes must be known before the utility of these molecules as reporter groups in biochemical systems can be

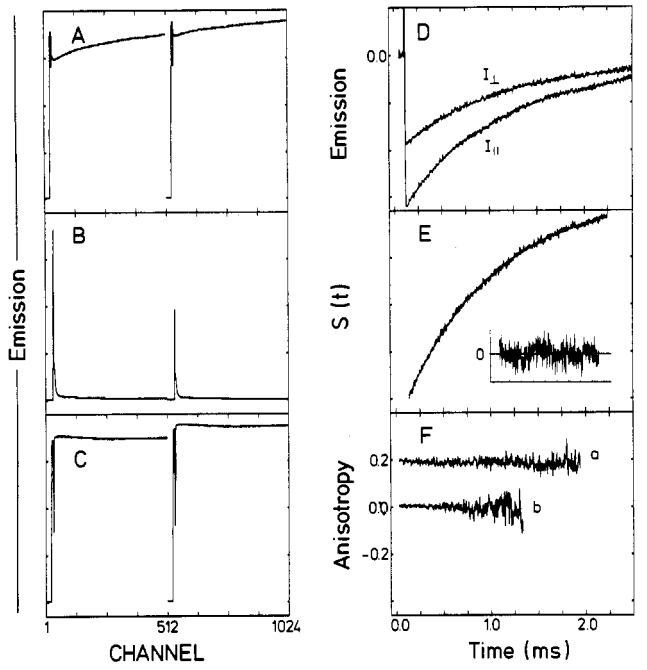

FIGURE 3: Fluorescence depletion of carboxyeosin in solid PMMA matrix. In traces A–C the parallel ($I_\parallel$) (channels 1–512) and perpendicular ($I_\perp$) (channels 513–1024) emission components are shown after 4096 data sweeps. (A) Depletion signals; (B) observed emission profiles with the actinic laser only; (C) steady-state fluorescence profiles (i.e., with only the CW argon laser); (D) polarized emission components after subtraction of curves B and C from curve A; (E) $S(t)$ curve and residuals plot (shown here and elsewhere with an expanded scale) with τ = 998 μs; (F) anisotropy profiles in (a) PMMA and (b) phosphate buffer. The smooth lines in this figure and other figures represent the results of computer analyses which are given in Table I. Experimental conditions were as follows: T = 6 °C; actinic laser energy = 0.18 mJ/pulse; monitoring laser power = 0.01 W; emission filters, KV550, dichromate solution, Corion 600-nm narrow band-pass; [CarEo] = 1.0 μM.

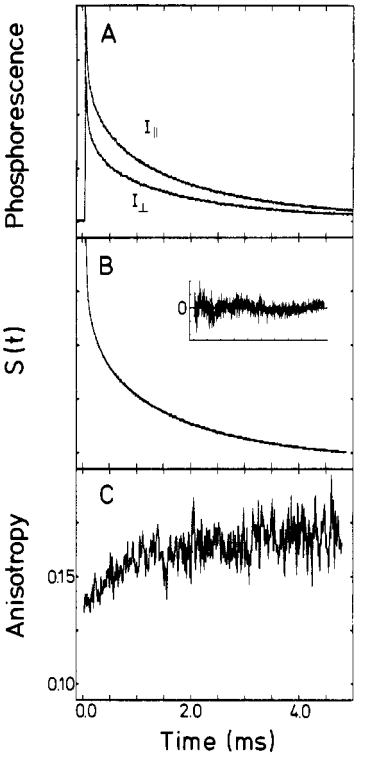

FIGURE 4: Phosphorescence of carboxyeosin in solid PMMA matrix: (A) polarized decay components; (B) total phosphorescence decay and residuals plot for a three-exponential fit; (C) anisotropy profile. A total of 4096 sweeps were collected. Experimental conditions: T = 6 °C; actinic laser energy = 0.18 mJ/pulse; emission filters, KV550, dichromate solution, RG645; [CarEo] = 1.0 μM.

assessed. Direct observation of the delayed emission (i.e., phosphorescence and delayed fluorescence) from probes with relatively large quantum yields for intersystem crossing to the triplet state Φ_t [eosin, Φ_t = 0.71; erythrosin, $\Phi_t \sim 1.0$ (Bowers & Porter, 1967)] provides a convenient means of measuring their spectral distribution, lifetimes, and initial anisotropies under a number of conditions [Jovin et al., 1981; Austin et al. (1979) and references cited therein]. However, the triplet states of other probes which exhibit very small intersystem crossing probabilities [fluorescein, Φ_t = 0.05 (Bowers & Porter, 1967); rhodamine, $\Phi_t \leq 0.05$ (Lessing & von Jena, 1967)] can only be monitored indirectly by observing depletion of the ground state (Johnson & Garland, 1981, 1982). Using fluorescence to monitor the ground state provides great sensitivity if the quantum yield for fluorescence emission Φ_f is appreciable. The sensitivity of direct detection of delayed luminescence is a function of Φ_t while the sensitivity of detection of the triplet state in FRS measurements is a function of the ratio Φ_f/Φ_t (Johnson & Garland, 1982; these authors have, in fact, used this ratio as a figure of merit in assessing a probe for FRS measurements). According to these criteria, it is clear that eosin [Φ_f = 0.16 (Forster & Livingston, 1952) and $\Phi_f/\Phi_t \sim 0.23$] is suitable for use in both methods while erythrosin [$\Phi_f \sim 0.02$ (Bowers & Porter, 1967; Lessing et al., 1976) and $\Phi_f/\Phi_t \sim 0.02$] should be a better phosphorescence probe than an FRS probe.

Comparison of FRS and Phosphorescence Measurements. Figure 3 shows typical FRS records, and the corresponding phosphorescence emission data are given in Figure 4. A number of features warrant comment. First, the FRS correction files generated with the CW argon laser alone show a rise in the gain immediately after the PMT gating pulse is applied that slowly decays with time (Figure 3C). This effect is caused by two separate factors which can be experimentally distinguished. If a scattering solution (Ludox) is used, the initial rise in gain is observed only if the PMT gating pulse is applied; there is no subsequent decay of the scattered light. The emission of the fluorophore ErITC observed in the absence of the gating pulse lacks the initial rise, but the subsequent slow decay remains. Thus, we attribute the initial instantaneous rise in gain to an electronic effect of the gating pulse on the photomultiplier response (gain) and the subsequent decay to the population of the triplet state due to steady-state excitation by the monitoring beam.

A theoretical analysis of the photochemical and instrumental processes contributing to the complete FRS measurement (see Appendix A) leads to the relation:

$$\Delta I(t) \propto -\Delta G(1 + \epsilon) \exp(-t/\tau') \quad (3)$$

where $\Delta I(t)$ is the intensity of either the parallel or perpendicular components as defined under Materials and Methods, $\Delta G = G_T - G_0$ where G_T is the total concentration of chromophore and G_0 is the ground-state concentration immediately after the depletion process, τ' is the apparent triplet-state lifetime, and ϵ is the fractional change in photomultiplier gain due to the gating. Under typical experimental conditions (e.g., in Figure 3C), ϵ is approximately +2.5% of the total steady-state signal and $1 > \tau'/\tau > 0.95$ (where τ is the true triplet-state lifetime; see Appendix A). A comparison between cases A and C of Figure 3 was made. For ErITC in PMMA, lifetimes of 301 and 344 μs were obtained, respectively, indicating that the same photophysical event is observed in both cases. Since case C involves excitation by the probe beam alone, such comparisons are possible only for fluorophores with

Table I: Summary of FRS and Phosphorescence Emission Decay Parameters

compd	concn[a] (μM)	conditions[b]	signal[c]	T (°C)	α_1	τ_1 (μs)	α_2	τ_2 (μs)	α_3	τ_3 (μs)	$\langle\tau\rangle$[d] (μs)	r_∞
CarEo	0.1	buffer	phos	6	0.08	140	0.92	321			306	0
	0.1	buffer	20%	6	1.0	288						0
	1.0	PMMA	phos	6	0.44	25	0.20	267	0.36	1803	713	0.15
	1.0	PMMA	20%	6	1.0	998						0.20
	1.0	arabinose	phos	6	0.14	92	0.86	428			381	0.20
ErITC	1.0	PMMA	phos	6	0.20	21	0.26	149	0.54	426	273	0.20
	1.0	PMMA	24%	6	1.0	301						0.22
EITC–conA	1–2	buffer	phos[e]	4	0.35	55	0.65	690			468	0
	0.25	buffer	15%	15	0.29	53	0.71	339			256	0
TMRITC–conA	1.0	buffer	10%	6	0.60	2398	0.40	10490			5635	0
		buffer	5%	15	1.0	3284						0
FITC–conA	1.0	buffer	10%	6	0.59	520	0.41	2344			1268	0
EITC–α_2M	0.26	buffer	phos	6	0.24	18	0.47	171	0.29	527	238	0
		buffer	20%	6	0.27	54	0.73	348			269	0
TMRITC–α_2M	0.23	buffer	10%	6	0.30	374	0.70	2432			1815	0
EITC–conA bound to A-431 cells	*f*	buffer	phos	6	0.40	17	0.28	100	0.32	471	186	0.05
	g	buffer	5%	6	0.38	16	0.62	274			176	0.09
	e	buffer	phos	4	0.46	22	0.54	350			199	0.05

[a] The numbers refer to luminescent probe concentrations. [b] Solution conditions were as follows: buffer, 5 mM sodium phosphate, pH 7.0; PMMA, solid matrix of poly(methyl methacrylate); arabinose, solid matrix composed of a racemic mixture of DL-arabinose. [c] Decay of the triplet state was monitored by phosphorescence emission (phos) or FRS; in the latter case the percent depletion is reported. [d] Average triplet-state lifetimes calculated according to $\langle\tau\rangle = \sum_{i=1}^{n}\alpha_i\tau_i$. [e] From Austin et al. (1979). [f] The cell concentration was 3×10^6 cells/mL. [g] The cell concentration was 1×10^6 cells/mL.

triplet quantum yields high enough so as to allow significant population by an argon laser. Under our experimental conditions, this was true only for erythrosin. The time course of both the FRS and phosphorescence measurements is determined by the lifetimes of all the species present. However, each amplitude term contributing to the total recovery of the fluorescence in FRS is determined only by the concentrations of the various triplet species; in contrast, the amplitudes in phosphorescence decay are also functions of the individual emission quantum yields of the triplet species present, which effectively act as weighting factors for the respective concentrations.

The photochemical properties of CarEo and ErITC were compared. From FRS measurements the triplet decay $S(t)$ of CarEo in PMMA is adequately fit to a single-exponential function (Figure 3E), in contrast to the corresponding phosphorescence experiment in which at least three exponential components were required for the analysis (Figure 4B, Table I). A similar behavior is observed for ErITC in PMMA; that is, a single exponential is sufficient for the FRS but not for the phosphorescence measurements (data not shown). Table I indicates that in general triplet lifetime data derived from FRS can be analyzed with simpler functions than those from the corresponding phosphorescence decays.

The simpler behavior of the triplet-state decay kinetics by the FRS method conceivably could result from the subtraction procedure used in the generation of the decay curves, as described under Materials and Methods, which might more efficiently eliminate systematic instrumental errors or the effects of probe bleaching than the corresponding blanks used for phosphorescence data. For example, in the latter case cyclooctatetraene (COT) has been used to scavenge the triplet state and quench the delayed luminescence (Jovin et al., 1981), thereby generating a subtraction data set containing only the prompt fluorescence and any PMT recovery response. However, this method is not generally applicable because the chromophore is not always accessible to COT and the addition of large concentrations (up to 5 mM) of the quencher to complex biochemical systems, e.g., whole cells, is highly undesirable.

It is also possible that the simpler decay processes for the FRS compared to the delayed luminescence method are apparent, i.e. reflect an inherently lower signal-to-noise ratio (SNR). (The largest contributing factor to the noise in FRS measurements made with our configuration is the 0.2% root mean square fluctuation of the CW argon laser.) The FRS measurements are intrinsically noisier than those of delayed luminescence because the signals are derived as differences corresponding typically to only 5–25% of the steady-state emission signal. In the case of phosphorescence or delayed fluorescence, excitation is only via a single initial light pulse and thus the emission signal is referenced to a negligible background level. In order to assess such effects, $S(t)$ curves were obtained with both methods by using 0.1 μM CarEo in phosphate buffer. Similar SNR ratios ($\sim$80) were achieved by adjusting the number of signal averages; 6 times as many cycles were necessary for the FRS experiment. Whereas good fits to a monoexponential function were obtained for $S(t)$ data measured by FRS, a multiexponential analysis was needed to represent the time course of phosphorescence. Thus, the different decay kinetics are not attributable to the selective SNR.

An immobilized chromophore should not exhibit a time-dependent depolarization of the emitted light on the microsecond to millisecond time scale. Studies conducted by Rutherford and Soutar (1977) show that the shortest correlation times reflecting the onset of segmental motion of poly(methyl methacrylate) at $\sim$0 °C occur in seconds. Therefore, a time-independent anisotropy profile in the submillisecond time range is expected for CarEo and ErITC in PMMA. This result is observed for both probes when FRS is used; the r_0 values are 0.20 and 0.22, respectively. However, $r(t)$ curves constructed from the polarized components of the phosphorescence decay show rising anisotropies: in the case of CarEo $r(t)$ rises in $\sim$200 μs from an $r(8) < 0.1$ to a limiting anisotropy r_∞ of 0.17; the corresponding values for ErITC are $r(8) < 0.13$ and $r_\infty = 0.19$. [$r(8)$ is the anisotropy 8 μs after the actinic pulse, i.e., after following the perturbing effects of high intensity prompt fluorescence.] The r values for both eosin and erythrosin in the PMMA solid matrix fall within the range previously reported for phosphorescence and fluorescence depletion methods [eosin, 0.18–0.3; EITC, 0.25 (Garland & Moore, 1979; Johnson & Garland, 1981)]. To determine whether the rising anisotropies derived from

phosphorescence are peculiar to the PMMA matrix, we measured the phosphorescence-decay of a solid matrix of a racemic mixture of DL-arabinose (Corin et al., 1985) doped with CarEo. The initial anisotropy $r(8)$ of <0.1 rises within 200 μs to a constant level of 0.2. Figure 9a,b in a previous report by Garland and Moore (1979) shows the time dependence of the polarized components of the phosphorescence emission for erythrosin and eosin in PMMA. A plot of the anisotropies constructed from their erythrosin data indicates a constant anisotropy of ~0.26 on the microsecond time scale. However, in the case of eosin, a rising anisotropy is apparent at early times.

A rationale for these phenomena is supplied by an analysis of the corresponding difference intensity function $d(t)$ constituting the numerator of $r(t)$. For example, in the case of CarEo in PMMA, $d(t)$ is resolved into a three-exponential decay with time constants within 10% of those obtained for $S(t)$. The relative amplitude of the middle component in $d(t)$ (ca. 0.27 ms), however, is only about $^1/_2$ that of the corresponding component in $S(t)$. The simplest interpretation is that, in phosphorescence, the three-component decay derives from the superposed contributions of three immobile species, one of which has about half the steady-state anisotropy of the other two. Thus, the resulting $r(t)$ function increases in the time period between the middle and slowest decays. It is possible that intermolecular complexes are the basis for this behavior, the effect on phosphorescence being more pronounced because of the complex orbital mixing involved in intersystem crossing, whereas the delayed fluorescence reflects only the properties of the singlet state.

The fluorescence anisotropy values reported here and in previous studies for eosin and erythrosin are lower than 0.4, the theoretical value expected for a randomly oriented immobilized population of an emitting chromophore with parallel emission and absorption dipoles. In order to check whether our values were being accurately reported, we determined the steady-state fluorescence polarization of the CarEo and ErITC PMMA blocks in our triplet-state spectrometer, using the CW laser as a steady-state excitation source, and compared these values with those measured in the SLM spectrofluorometer. The triplet spectrometer yielded steady-state anisotropies of 0.33 for CarEo and 0.29 for ErITC, which are in good agreement with the range 0.31–0.34 determined with the SLM fluorometer and a value of 0.33 for ErITC conjugated to bovine serum albumin reported by Garland and Moore (1979). The values obtained correspond to an angle between the absorption and fluorescence emission dipoles of 18–25°. According to eq 1, the predicted FRS r_0 values for such angles should be approximately 10% less than that obtained with the steady-state measurements for which r_0 is given by the expression $0.4P_2(\cos \delta_{AE})$.

The lower r_0 values observed in the FRS measurements (~0.2) are most probably the result of systematic depolarization effects. Thus, if due to imperfect alignment the monitoring beam interrogates volume elements that are not subjected to depletion by the actinic beam and therefore have zero anisotropy, the perceived fractional depletion signal will be reduced from its higher true value. Furthermore, to the degree that the latter corresponds to energy densities approaching saturation, the polarization (anisotropy) of the depletion signal will be less than that calculated for limiting intensities (eq 1). A more general expression accounting for an arbitrary extent of excitation (Szabo et al.,, unpublished results) predicts that the observed values in the FRS experiments would correspond to a fractional depletion of 0.4–0.7. However, the average

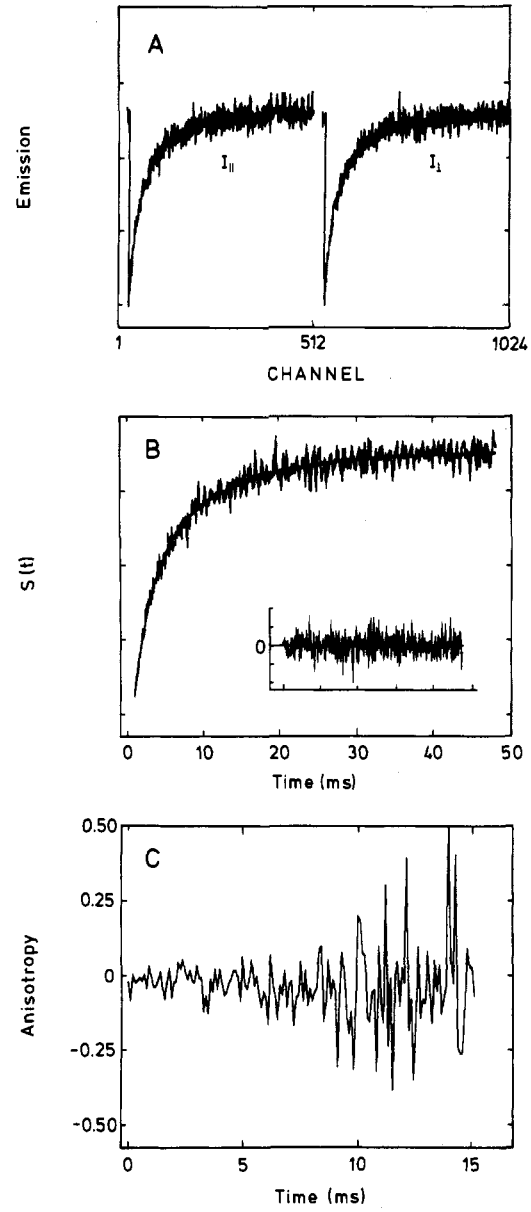

FIGURE 5: Fluorescence depletion of TMRITC–conA in phosphate buffer (3072 sweeps): (A) polarized components; (B) $S(t)$ profile and residuals plot; (C) anisotropy profile. Experimental conditions: [TMRITC] = 1.0 μM; 5 mM phosphate buffer, pH 7.0; T = 6 °C; actinic laser energy = 0.9 mJ/pulse; monitoring laser power = 0.06 W; emission filters same as in Figure 3.

apparent measured depletion was only about 0.2; this discrepancy would imply that $^1/_2$–$^2/_3$ of the monitored volume was not traversed by the actinic beam (assuming for simplicity homogeneous beam intensities).

FRS of Labeled Proteins and Applications. (A) Concanavalin A in Buffer. At pH 7.0 the 25 500-dalton polypeptide chains of conA form a tetramer (Wang et al., 1971). The predicted and experimentally obtained rotational correlation time in buffer is less than 1 μs (Austin et al., 1979), allowing measurement of triplet lifetimes under the experimental configuration adopted here. Figures 5 and 6 show the FRS data obtained for TMRITC–conA and FITC–conA, respectively, and Table I lists the lifetimes fitted according to eq 2 for all labeled conA derivatives. As expected, the anisotropy profiles generated in buffer are centered about the value 0. In most cases, two exponentials were required to adequately describe the $S(t)$ curves. An exception is TMRITC–conA at 15 °C for which a single exponential was sufficient. This result may be particularly useful in subsequent studies of protein

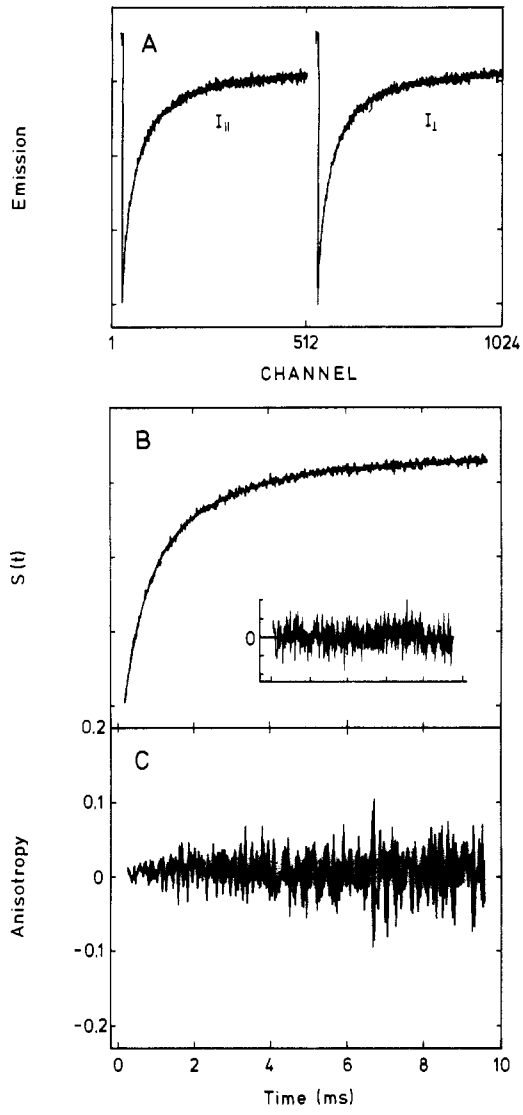

FIGURE 6: Fluorescence depletion of FITC–conA in phosphate buffer (3072 sweeps). The curves are defined as in Figure 5. Experimental conditions: same as in Figure 5 except actinic laser energy ≅ 1.8 mJ/pulse and monitoring laser power = 0.024 W.

rotations as multiple-exponential $S(t)$ decays complicate analyses of anisotropies. Another feature of the data is the extended time range available for the use of TMRITC and FITC; in the former case at 6 °C, the triplet-state emission process can be used for over 40 ms.

(B) α_2-Macroglobulin in Buffer. α_2M is an important proteinase inhibitor present in plasma and many tissues and consists of four identical polypeptide chains of M_r 180 000 (Sottrup-Jensen et al., 1984). In earlier fluorescence microscopy studies with fluorescein-labeled α_2M, pH changes were measured in endocytic vesicles containing α_2M (Tycko & Maxfield, 1982). However, no previous investigation involving the triplet state of labeled α_2M has been reported. As with conA, the rotational correlation time expected in buffer is less than 1 μs. Table I contains the fitted $S(t)$ curves for EITC–α_2M and TMRITC–α_2M. Two exponentials were required to adequately fit the FRS curves while, for EITC–α_2M, three exponentials were necessary for the phosphorescence measurement. However, the average lifetimes were similar, with $\langle\tau\rangle$ = 238 and 270 μs for the delayed emission and FRS measurements, respectively.

(C) Cells Labeled with EITC–ConA. In a previously published study of erythroleukemia cells labeled with eosin–conA (Austin et al., 1979), the anisotropy was shown to remain

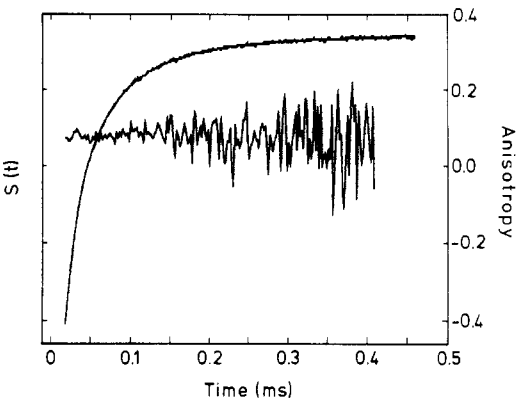

FIGURE 7: Fitted $S(t)$ curve and anisotropy profile for the FRS of EITC–conA bound to A-431 cells. Experimental conditions: the number of cells was adjusted to 2×10^6 cells/mL; the buffer was 5 mM phosphate, pH 7.0; T = 6 °C; actinic laser energy ≅ 0.9 mJ/pulse; monitoring laser power = 0.07 W; emission filters same as in Figure 3.

constant over the time range of triplet emission. This finding indicated the absence of significant global rotation of bound conA. In a similar manner, FRS measurements of EITC–conA bound to living human epidermoid carcinoma cells (A-431) were performed and compared with phosphorescence emission data. Figure 7 shows a fitted $S(t)$ curve and anisotropy profile from FRS measurements, and Table I lists the parameters obtained under a number of different conditions.

The residual anisotropy of r_∞ = 0.05 for the emission measurement is the same as that obtained by Austin et al. (1979). This value when compared with that for immobilized EITC ($r \sim 0.2$) indicates the existence of fast local motions of the eosin chromophore. Our FRS measurements give a higher value of r_0 = 0.09, probably due to the smaller angle between the emission and absorption dipoles for fluorescence as compared to phosphorescence. That is, the anisotropy values are intrinsically higher in FRS measurements. The constancy of the anisotropy supports the previous conclusion that no significant global rotation takes place in the time domain examined.

(D) I^- Quenching of EITC–ConA and TMRITC–ConA in Buffer. Fluorescence quenching measurements in membranes and proteins have been used extensively to investigate lipid and polypeptide dynamics and surface permeability (Eftink & Ghiron, 1981; Blatt & Sawyer, 1985). More recently, measurement of the triplet states of chromophores have found application for investigating quenching rate constants below 10^8 M^{-1} s^{-1} since the longer lifetimes offer greater sensitivity (Calhoun et al., 1983a,b; Barboy & Feitelson, 1985; Blatt & Corin, 1986). In this section, the suitability of the FRS method in quenching experiments is shown by presentation of I^- quenching of TMRITC–conA and EITC–conA.

The quenching results were subjected to two forms of analysis. In the first, the data were plotted (Figure 8A) according to the Stern–Volmer equation (Stern & Volmer, 1919; Lakowicz, 1983):

$$(\langle\tau_0\rangle/\langle\tau\rangle) - 1 = K[Q] = k_{q,app}\langle\tau_0\rangle[Q] \qquad (4)$$

where $\langle\tau_0\rangle$ and $\langle\tau\rangle$ are the average triplet-state lifetimes ($\langle\tau\rangle = \sum_{i=1}^{n}\alpha_i\tau_i$) in the absence and presence of quencher, respectively (see also Appendix B), K is the Stern–Volmer constant, and $k_{q,app}$ is the apparent bimolecular quenching rate constant assuming a quenching efficiency of unity (Eftink & Ghiron, 1981). The value of n was 2 and 1 for EITC–conA and TMRITC–conA, respectively. The data were also plotted (Figure 8B) according to a modified form of an equation

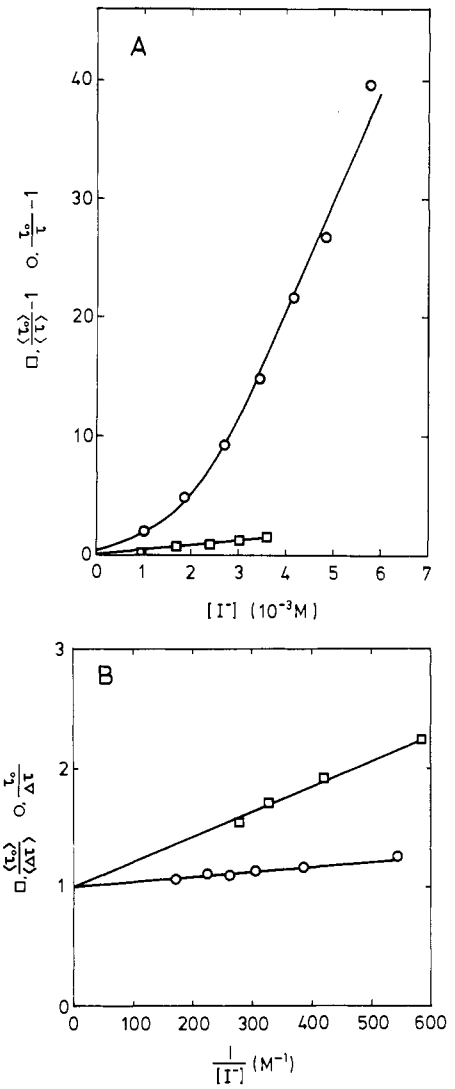

FIGURE 8: I^- quenching at 15 °C of the FRS of TMRITC–conA (○) and EITC–conA (□) in 5 mM phosphate buffer, pH 7.0: (A) Stern–Volmer plot (eq 4); (B) modified Lehrer plot (eq 5).

proposed by Lehrer (1971), where triplet-state lifetimes are used instead of steady-state fluorescence intensities (see Appendix B):

$$\langle\tau_0\rangle/\langle\Delta\tau\rangle = 1/[Q]f_a k_{q,app}\langle\tau_0\rangle + 1/f_a \qquad (5)$$

where f_a is the fraction of fluorophores accessible to the quencher and $\langle\Delta\tau\rangle = \langle\tau_0\rangle - \langle\tau\rangle$. Linear plots were obtained for EITC–conA with $f_a = 1$ and $k_{q,app} = 2.6 \times 10^6$ M^{-1} s^{-1}. In the case of TMRITC–conA, an upward curvature of the Stern–Volmer plot is observed at low quencher concentrations. From the linear region at higher $[I^-]$, the plot according to eq 5 was constructed and gave parameters of $f_a = 1$ and $k_{q,app} = 1.5 \times 10^6$ M^{-1} s^{-1}, in good agreement with the fitted parameters for EITC–conA.

A number of factors warrant consideration in the interpretation of the quenching data presented. First, the FRS measurement for eosin in buffer resulted in a single-exponential decay. The multiexponential decay observed when eosin is attached to the protein could arise from a heterogeneous population of probes according to eq B1 (see Appendix B). Some heterogeneity might still exist in the case of TMRITC–conA although monoexponential decays were obtained. The nonlinearity of the Stern–Volmer plot at low quencher concentration could be indicative of this possibility (Eftink & Ghiron, 1981).

The second consideration is the calculated values of $k_{q,app}$ which are 3–4 orders of magnitude less than that expected for diffusion-controlled bimolecular collisions in water. This result could arise from chromophores being buried deep within the protein matrix so that accessibility would be limited to the quencher diffusing through the protein matrix (Eftink & Ghiron, 1975, 1976, 1977). Alternatively, it could be the result of an intrinsically inefficient quenching mechanism. In order to distinguish between these two possibilities, the quenching of EITC by I^- in buffer was measured. A linear Stern–Volmer plot was obtained with $k_{q,app} = 1.5 \times 10^7$ M^{-1} s^{-1}. This value corresponds to an efficiency of $\gamma = 1.7 \times 10^{-3}$. ($\gamma$ is the probability that quenching occurs by collisions of probe and quencher.) Taking the value of γ into account gives $k_q = 1.5 \times 10^9$ M^{-1} s^{-1} for EITC–conA. This value is about $^1/_5$ the diffusion-controlled rate coefficient $k_{diff} = 8.4 \times 10^9$ M^{-1} s^{-1} calculated from the Stokes–Einstein relation with slip (Osborne & Porter, 1965) and can be compared with $k_q \sim 10^8$ M^{-1} s^{-1} obtained for the phosphorescence quenching by I^- of the buried tryptophan in alcohol dehydrogenase from horse liver (Barboy & Feitelson, 1985). As I^- is normally hydrated (Eftink & Ghiron, 1981) and the isothiocyanate derivatives of the water-soluble chromophores eosin and tetramethylrhodamine are known to conjugate with surface amino groups, collisions between probe and quencher probably occur by diffusion through water. This conclusion is substantiated by the calculated value of $f_a = 1$, which indicates that all probes are accessible to the quencher. Thus, the lower values of k_q compared to that expected for free diffusion in water are probably due to a negatively charged surface and/or probe environment at pH 7; the isoelectric point of the protein is <7 (Liener, 1976).

Summary and Conclusions

The principal aims of this study were to describe an experimental method for detecting the triplet states of fluorophores by the FRS technique and demonstrate its applicability to the study of biological systems. A brief summary of the suitability of FRS, a comparison to the phosphorescence emission method, and indications for further development are now presented.

Generally, the following factors warrant consideration in evaluating the applicability of an experimental technique: (i) accuracy; (ii) data acquisition time; (iii) expense associated with equipment and materials; (iv) advantages and disadvantages compared with other techniques that measure similar physical phenomena. First, we consider the accuracy of FRS as judged by comparison with the phosphorescence emission technique. In both cases a number of instrumental difficulties arise due to scattered light, prompt fluorescence, and the electronic gating of the photomultiplier (Bürkli & Cherry, 1981; this laboratory). The simpler analyses of $S(t)$ data and the concordance of observation with the predicted behavior for immobilized probes predicted for the FRS method suggest that this technique provides a more limited and/or more accurate representation of triplet-state decay processes.

The most obvious advantage of the FRS method is that it widens the scope of probes appropriate for the investigation of events in the microsecond to millisecond time range. For example, triplet-state emission of the halogen-substituted fluorescein derivatives, eosin and erythrosin, at temperatures above 4 °C generally does not last longer than 4 ms, in contrast to fluorescein and tetramethylrhodamine for which triplet emission processes were detected up to 40 ms (TMRITC). Such long triplet lifetimes provide an extended time domain in which quenching processes can be investigated. Also, for

TMRITC–conA in buffer at 15 °C a monoexponential $S(t)$ curve was observed, greatly simplifying interpretations of quenching and anisotropy data. A further potential advantage of the method is that it allows excitation of different transition directions in the label (Wegener, 1984) so as to better define the rotational motions of macromolecules, as shown for smaller molecules by using nanosecond fluorescence depolarization techniques (Barkley et al., 1981).

The practical disadvantages of FRS technique should be recognized. First, as compared to the phosphorescence emission technique, a second laser (in our configuration) and a number of additional optical accessories make the FRS more expensive and more complex. In order to obtain the necessary energy densities in the required time, a relatively powerful actinic laser is required. As a consequence, bleaching of the probe may be significant, although the effects can largely be accounted for by the collection sequence outlined under Materials and Methods. A second disadvantage of the FRS technique is the longer collection time. As shown in an earlier section, approximately 6 times as many sweeps are required in order to obtain the same SNR as with phosphorescence. (This comparison, of course, does not hold for nonphosphorescent probes.) Collection time is further lengthened by the need to record two blank subtract files rather than one.

A number of further developments are indicated from the work presented in this paper. First, incorporation of the instrumental configurations suggested by Wegener (1984) and Szabo et al. [unpublished results; see also Yoshida and Barisas (1986)] will allow lifetime and anisotropy measurements for the general case. Second, in the course of this study it was discovered that the triplet state of erythrosin can be populated to a significant extent by irradiation with the argon laser alone, an effect that can be exploited for lifetime measurements by phosphorescence with this and related chromophores by using rapid shuttering with the electrooptic modulator. Finally, the two-laser configuration may be adaptable to the microscope, thus allowing better time resolution than with previously adopted configurations (Johnson & Garland, 1981, 1982) in which the required bleaching pulse using the single argon laser is longer than many kinetic and rotational depolarization processes of interest (Corin et al., 1985).

Appendix

(A) Photochemical and Instrumental Contributions to FRS. We begin by considering the processes affecting the concentration of ground-state chromophores G, and triplet-state chromophores T, immediately after the δ excitation of the actinic laser, which we define as occurring at $t = 0$. The total concentration of ground-state chromophores is given by

$$G_T = G_0 + T_0 \tag{A1}$$

Thereafter, the ground state is depleted by the monitoring beam with a rate constant k_e and is repopulated by decay from the triplet state with a rate constant k_d. We assume k_e and k_d are both first-order rate coefficients. Since $G_T = G + T$

$$dG/dt = k_d G_T - (k_e + k_d)G \tag{A2}$$

We let $\tau = 1/k_d$ and $\tau' = 1/(k_e + k_d)$, which gives

$$G(t) = (\tau'/\tau)G_T + [G_0 - (\tau'/\tau)G_T] \exp(-t/\tau') \tag{A3}$$

We now consider the photochemical and instrumental contributions occurring for each of the three data-collection modes outlined under Materials and Methods and shown experimentally in Figure 3A–C. The measured signal $I(t)$ can be resolved into components due to steady-state fluorescence ($s1$), delayed emission ($s2$: phosphorescence, delayed fluorescence), incompletely gated prompt fluorescence transient ($s3$), and electronic offset ($s4$). Due to the different spectral distribution of the delayed emission (in the case of phosphorescence) we assign to $s2$ a sensitivity δ relative to that for fluorescence. The gating function leads to a time-dependent change in photomultiplier gain $\alpha(t)$ (applicable to $s1$, $s2$, and $s3$) and an additional factor $\beta(t)$ in the case of $s3$. In case A (both lasers)

$$\begin{aligned} s1 &= \{(\tau'/\tau)G_T + [G_0 - (\tau'/\tau)G_T] \exp(-t/\tau')\}\ \alpha(t) \\ s2 &= (G_T - G_0)\ \alpha(t)\ \delta \exp(-t/\tau) \\ s3 &= G_T\ \beta(t)\ \alpha(t) \end{aligned} \tag{A4}$$

In case B (actinic laser only), $s1 = 0$, and $s2$ and $s3$ are the same as in case A. In case C (monitoring laser only), $s2 = s3 = 0$, and

$$s1 = G_T[(\tau'/\tau) + (1 - \tau'/\tau) \exp(-t/\tau')]\ \alpha(t) \tag{A5}$$

The offsets $s4$ are assumed to be different for the three cases but constant before and after the actinic pump. In cases A and C, $s1 = G_T$ before the actinic pump but obviously equals 0 for case B.

Subtraction of $I(t)$ for cases B and C from that for case A and formation of the difference to the combined signal prior to the actinic pump lead to

$$\Delta I(t) \propto -\Delta G\ \alpha(t) \exp(-t/\tau') \tag{A6}$$

where $\Delta G = G_T - G_0$. In the case that $\alpha(t)$ is given by $(1 + \epsilon)$, i.e., reflecting a constant perturbation in electronic gain, eq A6 reduces to the single-exponential expression given by eq 3 under Results and Discussion. Note that the effect of any arbitary $\alpha(t)$ cancels out in the calculation of $r(t)$.

(B) Modified Lehrer Equation. We consider the case where a probe is located in n different environments and each probe is characterized by a unique triplet-state lifetime reflecting the properties of that environment. In the absence of quencher, the decay of the triplet state may be represented by

$$I_0(t) \propto \alpha_{0,1} \exp(-t/\tau_{0,1}) + \alpha_{0,2} \exp(-t/\tau_{0,2}) + \ldots + \alpha_{0,n} \exp(-t/\tau_{0,n}) \tag{B1}$$

where $\alpha_{0,i}$ is the fractional contribution of lifetime component τ_i. Similarly, in the presence of quencher

$$I(t) \propto \alpha_1 \exp(-t/\tau_1) + \alpha_2 \exp(-t/\tau_2) + \ldots + \alpha_n \exp(-t/\tau_n) \tag{B2}$$

Ideally, the quenching efficiency of each component i will be determined by comparing the value of τ_i to $\tau_{0,i}$. Experimentally, it is difficult to resolve multiple-component decays, especially when lifetimes are similar. Moreover, in quenching experiments amplitudes and lifetimes change, depending on the quenching efficiency and accessibility of each component. In order to simplify the analysis, we define average lifetimes:

$$\begin{aligned} \langle \tau_0 \rangle &= \sum_{i=1}^{n} \alpha_{0,i}\tau_{0,i} \\ \langle \tau \rangle &= \sum_{i=1}^{n} \alpha_i\tau_i = \sum_{i=1}^{n} \alpha_{0,i}\tau_{0,i}/(1 + K_i[Q]) \end{aligned} \tag{B3}$$

in the absence and presence of quencher, respectively. K_i is the Stern–Volmer constant associated with the quenching of each $\tau_{0,i}$. The convenient ratio $\langle \tau_0 \rangle/(\langle \tau_0 \rangle - \langle \tau \rangle)$ is given by

$$\langle \tau_0 \rangle / \langle \Delta\tau \rangle = \{\sum_{i=1}^{n} f_i K_i[Q]/(1 + K_i[Q])\}^{-1} \tag{B4}$$

where $f_i = (\alpha_{0,i}\tau_{0,i})/\langle \tau_0 \rangle$. If we assume there are m accessible probes with the same value of K and $n - m$ inaccessible probes with $K = 0$

$$\langle\tau_0\rangle/\langle\Delta\tau\rangle = 1/(f_aK[Q]) + 1/f_a \quad \text{(B5)}$$

where $f_a = \sum_{i=1}^{m} f_i$. A plot of $\langle\tau_0\rangle/\langle\Delta\tau\rangle$ against $1/[Q]$ is linear and allows determination of f_a and K from the intercept and slope, respectively. Equation B5 is similar to that derived by Lehrer (1971) except it is expressed in terms of excited-state lifetimes rather than steady-state intensities. It has the advantage of monitoring only dynamic interactions and will not be influenced by any contributions of a static quenching mechanism.

Registry No. CarEo, 107175-26-8; ErITC, 72636-42-1; I^-, 20461-54-5.

References

Austin, R. H., Chan, S. S., & Jovin, T. M. (1979) *Proc. Natl. Acad. Sci. U.S.A. 76(11)*, 5650–5654.

Barboy, N., & Feitelson, J. (1985) *Photochem. Photobiol. 41*, 9–13.

Barkley, M. D., Kowalczyk, A. A., & Brand, L. (1981) *J. Chem. Phys. 75*, 3581–3593.

Blatt, E., & Sawyer, W. H. (1985) *Biochim. Biophys. Acta 822*, 43–62.

Blatt, E., & Corin, A. F. (1986) *Biochim. Biophys. Acta 857*, 85–94.

Bowers, P. G., & Porter, G. (1967) *Proc. R. Soc. London, A 299*, 348–353.

Bretscher, M. (1973) *Science (Washington, D.C.) 181*, 622–629.

Bürkli, A., & Cherry, R. J. (1981) *Biochemistry 20*, 138–145.

Calhoun, D. B., Vanderkooi, J. M., Woodrow, G. V., III, & Englander, S. W. (1983a) *Biochemistry 22*, 1526–1532.

Calhoun, D. B., Vanderkooi, J. M., & Englander, S. W. (1983b) *Biochemistry 22*, 1533–1539.

Chan, S. S., Arndt-Jovin, D. J., & Jovin, T. M. (1979) *J. Histochem. Cytochem. 27*, 56–64.

Cherry, R. J. (1978) *Methods Enzymol. 54*, 47–64.

Cherry, R. J. (1979) *Biochim. Biophys. Acta 559*, 289–327.

Corin, A. F., Matayoshi, E. D., & Jovin, T. M. (1985) in *Spectroscopy and the Dynamics of Molecular Biological Systems* (Bayley, P. M., & Dale, R. E., Eds.) pp 53–78, Academic, London.

Eftink, M. R., & Ghiron, C. A. (1975) *Proc. Natl. Acad. Sci. U.S.A. 72*, 3290–3294.

Eftink, M. R., & Ghiron, C. A. (1976) *Biochemistry 15*, 672–680.

Eftink, M. R., & Ghiron, C. A. (1977) *Biochemistry 16*, 5546–5551.

Eftink, M. R., & Ghiron, C. A. (1981) *Anal. Biochem. 114*, 199–227.

Förster, L. S., & Livingston, R. (1952) *J. Chem. Phys. 20*, 1315–1320.

Garland, P. B., & Moore, C. H. (1979) *Biochem. J. 183*, 561–572.

Garland, P. B., & Johnson, P. (1985) in *Spectroscopy and the Dynamics of Molecular Biological Systems* (Bayley, P. M., & Dale, R. E., Eds.) pp 95–118, Academic London.

Hoogevest, P., Kruijff, B., & Garland, P. B. (1985) *Biochim. Biophys. Acta 813*, 1–9.

Johnson, P., & Garland, P. B. (1981) *FEBS Lett. 132*, 252–256.

Johnson, P., & Garland, P. B. (1982) *Biochem. J. 203*, 313–321.

Jovin, T. M., Bartholdi, M., Vaz, W. L. C., & Austin, R. H. (1981) *Ann. N.Y. Acad. Sci. 366*, 176–196.

Lakowicz, J. R. (1983) *Principles of Fluorescence Spectroscopy*, Plenum Press, New York.

Lehrer, S. S. (1971) *Biochemistry 10*, 3254–3263.

Lessing, H. E., & von Jena, A. (1979) in *Laser Handbook* (Stitch, M. L., Ed.) pp 753–846, North-Holland, Amsterdam.

Liener, I. E. (1976) in *Concanaval A as a Tool* (Bittiger, H., & Schnebli, H. P., Eds.) pp 17–31, Wiley, New York.

Matayoshi, E. D., Corin, A. F., Zidovetzki, R., Sawyer, W. H., & Jovin, T. M. (1983) in *Mobility and Recognition in Cell Biology* (Sund, H., & Veeger, C., Eds.) pp 119–134, de Gruyter, Berlin and New York.

Osborne, A. D., & Porter, G. (1965) *Proc. R. Soc. London, A 284*, 9–15.

Parker, C. A. (1968) in *Photoluminescence of Solutions*, p 267, Elsevier, Amsterdam.

Rigler, R., & Ehrenberg, M. (1976) *Q. Rev. Biophys. 9*, 1–19.

Rutherford, H. & Soutar, I. (1977) *J. Polym. Sci. 15*, 2213–2225.

Sottrup-Jensen, L., Stepanik, T. M., Kristensen, T., Wierzbicki, D. M., Jones, C. M., Lonblad, P. B., Magnusson, S., & Petersen, T. E. (1984) *J. Biol. Chem. 259*, 8318–8327.

Stern, V. O., & Volmer, M. (1919) *Phys. Z. 20*, 183–189.

Tycko, B., & Maxfield, F. R. (1982) *Cell (Cambridge, Mass.) 28*, 643–651.

Wang, J. L., Becker, J. W., Reeke, J. N., Jr., & Edelman, G. M. (1971) *Proc. Natl. Acad. Sci. U.S.A. 68*, 1130–1134.

Wegener, W. A. (1984) *Biophys. J. 46*, 795–803.

Wegener, W. A., & Rigler, R. (1984) *Biophys. J. 46*, 787–793.

Yoshida, T. M., & Barisas, B. G. (1986) *Biophys. J. 50*, 41–53.